Check for updates

JGR Oceans

RESEARCH ARTICLE
10.1029/2022JC019338

Effect of Freshwater Discharge From Estuary Dam on Residual Circulation in Bifurcated Channel

J. W. Kim[1], J. I. Song[2], B. I. Yoon[2], and S.-B. Woo[3]

[1]Artificial Intelligence Convergence Research Center, Inha University, Incheon, Republic of Korea, [2]Gyeong·Incheon Sea Grant Center, Inha University, Incheon, Republic of Korea, [3]Department of Ocean Sciences, Inha University, Incheon, Republic of Korea

Key Points:

- Multi-layer vertical residual structure is due to induction of upstream residual flow from a narrow bifurcated channel
- Nonlinear effects occur at the bifurcation point of the channels
- The advection term dominated during non-discharge periods, whereas the vertical friction term dominated during discharge periods

Supporting Information:

Supporting Information may be found in the online version of this article.

Correspondence to:

S.-B. Woo,
sbwoo@inha.ac.kr

Citation:

Kim, J. W., Song, J. I., Yoon, B. I., & Woo, S.-B. (2023). Effect of freshwater discharge from estuary dam on residual circulation in bifurcated channel. *Journal of Geophysical Research: Oceans*, *128*, e2022JC019338. https://doi.org/10.1029/2022JC019338

Received 5 OCT 2022
Accepted 5 MAY 2023

Author Contributions:

Conceptualization: J. W. Kim, B. I. Yoon, S.-B. Woo
Data curation: J. W. Kim
Formal analysis: J. W. Kim, J. I. Song
Investigation: J. W. Kim, J. I. Song, S.-B. Woo
Methodology: J. W. Kim, J. I. Song, B. I. Yoon, S.-B. Woo
Project Administration: S.-B. Woo
Resources: J. W. Kim
Software: J. W. Kim
Supervision: S.-B. Woo
Validation: J. W. Kim
Visualization: J. W. Kim
Writing – original draft: J. W. Kim, S.-B. Woo
Writing – review & editing: J. W. Kim, J. I. Song, B. I. Yoon, S.-B. Woo

© 2023. American Geophysical Union. All Rights Reserved.

Abstract The residual structure of the inner part of the Yeongsan River estuary has been reported to be a multi-layer vertical structure, unlike the two-layer vertical structure of a typical estuary, due to irregular freshwater discharge. The inner estuary has a main channel connected to the open sea, and a bifurcated channel system (sub-channel) in its central part, which can affect the residual current. In this study, field observations of three-dimensional velocity and salinity were conducted to understand the discharge effects on the residual current at bifurcated channels. The residual flows were estimated using least-squares harmonic analysis. The relative contributions of advection acceleration and friction terms to nonlinear effects were evaluated using along-channel momentum balance. In the absence of freshwater discharge, the flow patterns were dominated by tidal dynamics in the sub-channel rather than the main channel, whereas most flow patterns during freshwater discharge were dominated by near-surface strong velocity in the main channel. A multi-layer vertical residual structure was observed during the non-discharge period in the main channel, which was caused by the insertion of upstream residual flow from the sub-channel. Nonlinear effects occurred at the bifurcation point of the two channels. During the non-discharge period, the advection term was most dominant, whereas the vertical friction term was dominant during the discharge period. Moreover, the magnitude of the horizontal friction term was larger than that of the advection term. Therefore, freshwater discharge can lead to an increase in the friction term, which in turn can markedly affect the residual circulation.

Plain Language Summary Residual circulation is a common and influential process in the major estuaries and coastal regions of the world, and understanding this is of great significance with respect to marine material transport, water quality, and ecological processes. The tidal propagation and residual flow patterns through the bifurcated narrow channel of the inner part of the Yeongsan River estuary are connected to the center of the main channel, which can significantly contribute to the formation of a vertical residual flow structure. Residual circulation shows a noticeable change due to the strong flow caused by the freshwater discharge from the estuary dam. Nonlinear effects occurred largely at the bifurcation point of the two channels, and in this regard, the major mechanisms of residual circulation differed between the two channels. Channel bifurcations are artificially or naturally formed along various coasts, and our research results provide a good example of identifying the causes of environmental changes.

1. Introduction

Residual circulation in estuaries is an important process for the distribution and movement of salt, sediment, pollutants, and plankton (Chen et al., 2009). Particularly in tidal-dominated estuaries, the instantaneous fluxes of materials are generated by flood and ebb currents, but the net exchange is predominantly determined by residual current patterns induced by tidal asymmetry, freshwater discharge, wind, and topography (Aubrey & Speer, 1985; Huijts et al., 2009). Therefore, understanding the spatiotemporal patterns of residual currents and their major controlling factors is an important consideration in the long-term management of the estuarine environment.

Most prior studies on the residual circulation have been conducted in natural estuaries, and classical theories were presented on the basis of studies in the Hudson River estuary (Dyer, 1997). In studies of the two-layer structure of residual circulation, it has been shown that seaward outflow at the surface layer is induced by the barotropic pressure gradient, while the landward inflow of more saline water near the bottom layer is induced by the baroclinic pressure gradient (Geyer et al., 2000). Hansen and Rattray (1965) successfully predicted the strength of residual circulation using the linear theory that the residual estuarine circulation is controlled by the balance

between horizontal pressure gradient and stress divergence. However, this linear theory has been challenged by several studies that show the influence of nonlinear advection, tidal asymmetry, uneven water depth distribution, and bottom frictional effects associated with topographic structures on residual circulation (Lacy et al., 2003; Trowbridge et al., 1999).

Residual circulation is also significantly influenced by the anthropogenic effects of marine infrastructure built to promote human activity. Controlled discharge of water from structures such as sea dikes, dams, tidal power plants, and estuary dams can cause greater flow changes than those in a natural estuarine system (Wu et al., 2017). In particular, when the flow related to water discharge is separated owing to differences in topographic shape, width, length, and depth distribution between multi-channels, the residual circulation mechanisms in the surrounding regions may vary owing to strong velocity shear and secondary flow (Buschman et al., 2010; Kim & Voulgaris, 2005). Furthermore, high freshwater discharge and suspended sediments can be asymmetrically transported by two or more channels during flooding seasons, which has a huge impact on delta formation in downstream areas, and requires an understanding of residual circulation in the bifurcated channels (Kästner & Hoitink, 2019; Zhang et al., 2017).

The Yeongsan River estuary system in South Korea is heavily influenced by the controlled discharge of freshwater through an estuary dam, and this discharged freshwater flow is bifurcated through multi-channels, interacting with the flow of the open sea. The controlled discharge from the estuary dam results in the sediments accumulated within Lake Yeongsan being very strongly discharged into the estuary over a short-term period, which markedly affects the residual circulation and mass transport (Park et al., 2001). For instance, the vertical structure of the water temperature in the Yeongsan River estuary exhibits a multi-layer structure owing to this irregular freshwater discharge (Cho et al., 2004), rather than the two-layer circulation structure found for any typical estuary. As the tidal current is blocked by the estuary dam, the magnitude of the current velocity decreases to less than half, and the residence time of near-bed materials increases owing to the strengthening of stratification (Kang, 1999; Kim et al., 2017). Various studies have been conducted in the Yeongsan River estuary to examine the causes of these changes. However, these studies have been mainly conducted using mooring observations, and analysis has been focused only on the main channel among the two channels connected to the open sea. As a result, questions regarding the spatiotemporal residual patterns of the secondary channels and their respective mechanisms remain unanswered.

In this study, a field survey of the three-dimensional flow pattern, water temperature, and salinity changes was performed on the bifurcated channel in the Yeongsan River estuary, and the effect of freshwater discharge on the residual circulation in each of the multi-channel was analyzed using these data. The objectives of this study were (a) to compare the spatiotemporal flow patterns and changes in salinity distribution between multi-channels during discharge and non-discharge periods, (b) to elucidate the structure of the residual flow, and (c) to estimate the major mechanism of residual circulation using momentum balances.

2. Study Area

The Yeongsan River estuary is located in the Mokpo region in the southwestern part of South Korea and consists of hundreds of intricately scattered islands as part of the topography (Figure 1a). The tides exhibit a typical semi-diurnal cycle with spring-neap variations, and the mean spring and neap tidal ranges are approximately 4 and 3 m, respectively. The water depth varies from approximately 2–50 m, and the mean depth is approximately 19 m. The tidal current propagates upstream through various channels between large and small islands such as Anjwado, Aphaedo, and the Hwawon Peninsula, but the water exchange between Lake Yeongsan and the estuary is artificially blocked by the estuary dam.

The inner part of the Yeongsan River estuary comprises a main channel in the east-west direction and a sub-channel in the north-south direction, both of which are connected to the open sea based on Mokpo Port (Figure 1b). The width of the main channel is 1–2 km, whereas the width of the narrower sub-channel is less than 1 km. The water depth of the main channel remains at almost 20 m throughout, but for a slope that changes rapidly from 20 to 8 m near the estuary dam due to frequent dredging. The water depth of the sub-channel varies from 10 to 22 m at the junction with the main channel and decreases to about 13 m at the entrance of the sub-channel to the open sea.

The Yeongsan estuary dam in the eastern part of Mokpo Port was built in February 1981 to secure agricultural water and prevent flooding (Figure 1c). The length of the dam is 4.35 km, and eight sluice gates for discharging

21699291, 2023, 5, Downloaded from https://agupubs.onlinelibrary.wiley.com/doi/10.1029/2022JC019338 by Inha University, Wiley Online Library on [11/03/2024]. See the Terms and Conditions (https://onlinelibrary.wiley.com/terms-and-conditions) on Wiley Online Library for rules of use; OA articles are governed by the applicable Creative Commons License

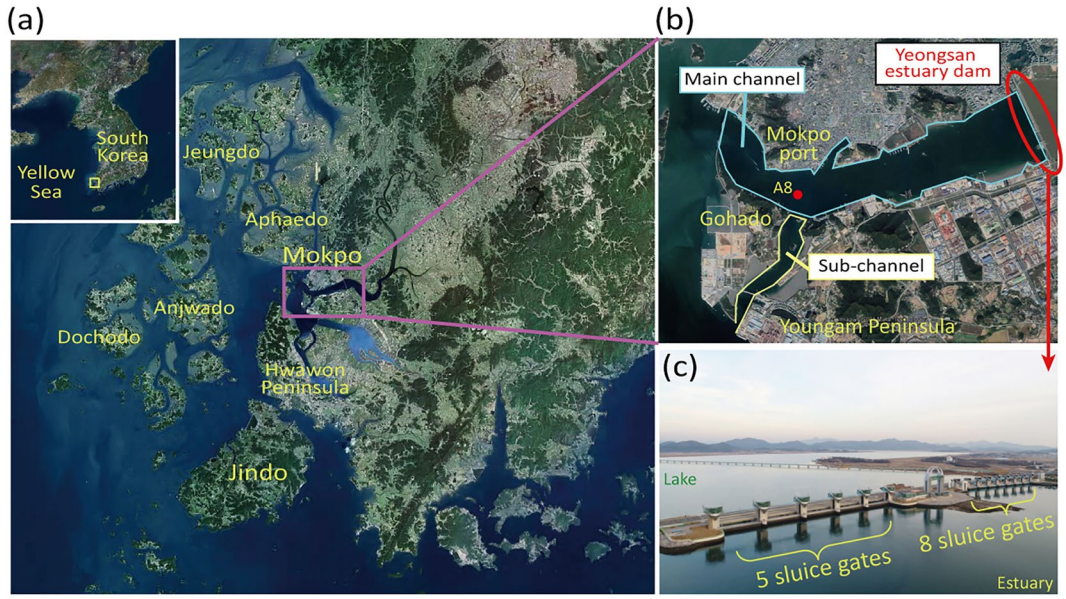


Figure 1. (a) Map showing the Yeongsan River estuary in the southwestern part of the Korean Peninsula. (b) The inner part of the estuary (pink square box) has two channels connected to the open sea in the western (main channel) and southern parts of Mokpo port (sub-channel), respectively. (c) The water exchange between Lake Yeongsan (upstream region of the estuary dam) and the estuary has been artificially blocked by the estuary dam (red ellipse).

freshwater toward the estuary are installed at the southern end of the dam. The water level in Lake Yeongsan, located upstream of the estuary dam, should be maintained at a specific water level 1 m lower than the mean sea level (MSL) of 0 m at Mokpo tide station due to the risk of flooding. When the water level difference between the lake and estuary reaches 2 m, and the specific water level in the lake (e.g., MSL. −1 m) is exceeded, the sluice gates are opened to discharge freshwater into the estuary. The total monthly volumes of freshwater discharged from the estuary dam from 1997 to 2011, obtained from the Yeongsan River estuary dam management center, are shown in Figure 2. The freshwater discharge almost always occurs in summer. Over 15 years, the median values between July and September varied from 3.84 to 4.51 $\times 10^8$ m^3, but were approximately four times lower at 0.31–1.18 $\times 10^8$ m^3 for the rest of the period. The volumes of freshwater discharged in May, July, and November 2011 were each higher than the median values for 15 years, while little freshwater discharge was performed during September. The volume of freshwater discharged in August, the observation period of this study, was comparable to the median value for 15 years. These high discharges from the estuary dam in summer indicate that the sediments accumulated in Lake Yeongsan are strongly discharged only during a specific period of 3 months each year, and most dynamic changes in the estuarine environment of the Yeongsan River likely occur during the summer.

The freshwater discharged from an estuary dam bifurcates at the junction (A8 in Figure 1) of the main channel and sub-channel. To quantify the freshwater partition at A8, the freshwater transports ($F = \int v(S_{ref} - S)/S_{ref} dz$) were estimated by using the salt-based method (Shan et al., 2019), where v is the observed normal velocity at A8 to the main channel and sub-channel, S_{ref} is 31.5 as the reference salinity, S is observed salinity at A8. Unlike Shan et al. (2019), this study cannot reflect the cross-sectional area, so the unit of freshwater transport is m^2 s^{-1}. The salinity and velocity data at A8 used the data obtained during the neap tide of this study, and the methods and results are described in Sections 3.1 and 4.2, respectively. As a result, the freshwater transport is approximately 1.5 times greater toward the main channel than the sub-channel (N7–N11 in Figure 2b). In percentage, about 56%–65% of freshwater escapes toward the main channel, and about 34%–43% of freshwater escapes toward the sub-channel.

The effect of the Earth rotation on the freshwater plume in the Yeongsan River estuary was insignificant. To examine the influence of the Earth rotation on the freshwater plume in the Yeongsan River estuary, the Rossby internal radius of deformation ($R_0 = \sqrt{g'H}/f$) is estimated by the equation presented in Shan et al. (2019), where H is the upper layer depth of the stratification, f is the Coriolis parameter, and the $g' = g(\rho_2 - \rho_1)/\rho_1$ is the

21699291, 2023, 5, Downloaded from https://agupubs.onlinelibrary.wiley.com/doi/10.1029/2022JC019338 by Inha University, Wiley Online Library on [11/03/2024]. See the Terms and Conditions (https://onlinelibrary.wiley.com/terms-and-conditions) on Wiley Online Library for rules of use; OA articles are governed by the applicable Creative Commons License

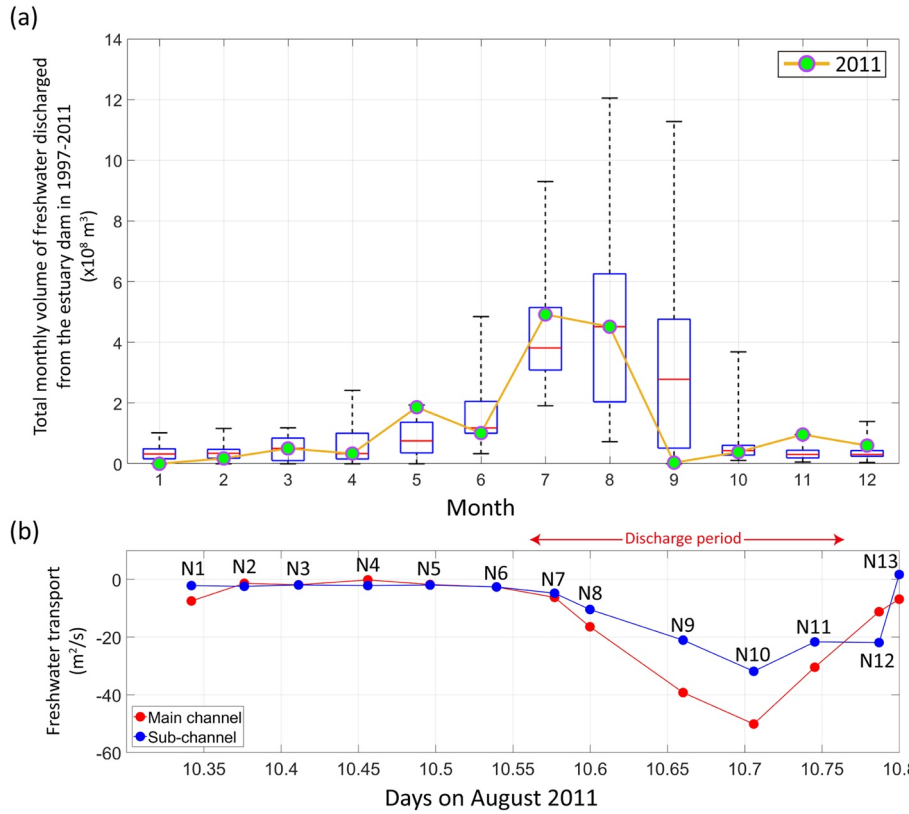


Figure 2. (a) Statistical analysis of the total monthly volume of freshwater discharged from the estuary dam from 1997 to 2011. In (a), the solid yellow line with circle symbols represents the monthly total monthly volume of freshwater discharged in 2011. (b) Salt-based estimate of freshwater transport for the main channel (red solid line) and sub-channel (blue solid line) at A8.

reduced gravity. ρ_1 and ρ_2 are the average densities of the upper and lower layers of the stratification, respectively. H, ρ_1, and ρ_2 were defined based on the salinity results of this study at A8. This will be described in more detail in Section 4.2 (e.g., Figure 7). H was defined as 10 m because a decreasing salinity gradient from 30 to 0 was measured at water depths of 0–10 m, while the salinity profile at depths of 10–23 m was vertically homogeneous at about 30 during the freshwater discharge. At the time-averaged density profile (thick black solid line in Figure S1 in Supporting Information S1), ρ_1 and ρ_2 are 1,011 and 1,020 kg m^{-3}, respectively. f is 8.32×10^{-5} s^{-1} at the latitude of 34.7°N. The estimated R_0 in the Yeongsan River estuary was approximately 11 km. Considering that the width of the main channel and the sub-channel is 1–2 km, the impact of the Earth's rotation on the freshwater plume dynamics in this region may be negligible. Therefore, it can be expected that the freshwater is moved not only to the main channel but also to the sub-channel due to advection or vertical stress rather than the influence of the Earth's rotation.

3. Materials and Methods

3.1. Data Collection and Processing

To investigate the flow characteristics associated with discharge impacts in the frontal regions of the Yeongsan estuary dam in August 2011, spatiotemporal current velocity, salinity, and water temperature data were collected along lines A1–A7 and B5–B1(A8)–A10 using two vessels (Figure 3a). To compare the flow interaction between the two channels, the observation lines of A1–A10 and B1–B5 were defined as transects I and II, respectively. Note that there is no data between A7–A8 because the investigation has not been conducted. Surveys were conducted on August 10 and August 15 at 1 hr intervals for a total of 13 hr, and three-dimensional velocity data were collected using bottom tracking modes of acoustic Doppler current profiles (ADCP, RDI 600 kHz) fixed to the ship's frame (Table 1). The ADCP was installed at 0.8 m below the water surface, and the blanking distance

21699291, 2023, 5, Downloaded from https://agupubs.onlinelibrary.wiley.com/doi/10.1029/2022JC019338 by Inha University, Wiley Online Library on [11/03/2024]. See the Terms and Conditions (https://onlinelibrary.wiley.com/terms-and-conditions) on Wiley Online Library for rules of use; OA articles are governed by the applicable Creative Commons License

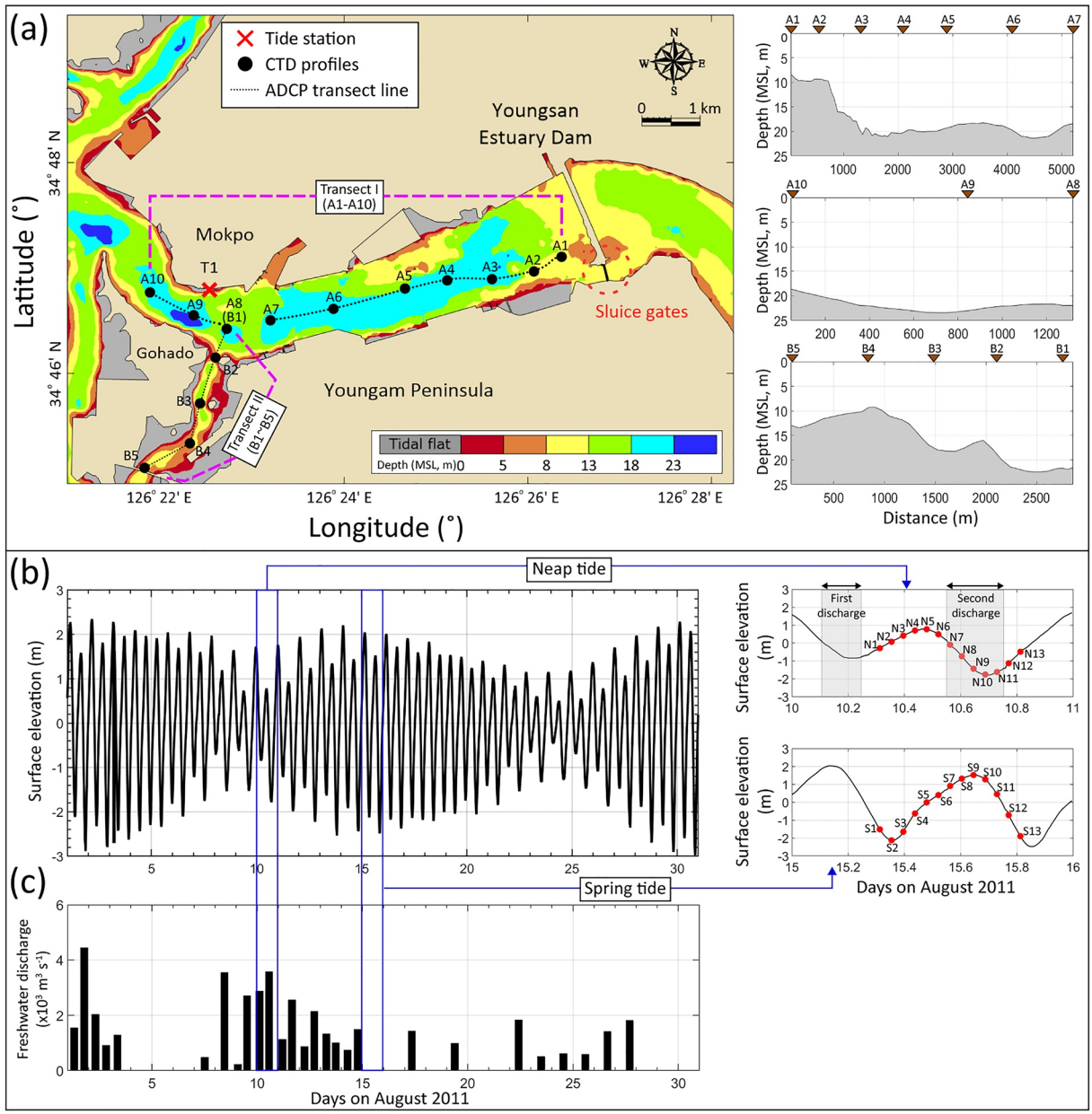


Figure 3. (a) Location of the acoustic Doppler current profiles transect lines and conductivity-temperature-depth profiles in the inner part of the Yeongsan River estuary. The spatial water depth distribution is expressed as contours, and cross-sectional views for the water depths of three lines, A7–A1, A8–A10, and B1–B5 are also presented. (b) Time series of the surface elevation during August 2011. Two-time windows of 10 and 15 days were selected to represent the observation times and water level variations during the neap and spring tides, respectively. (c) Freshwater discharge rate from the estuary dam.

was set to 1 m. The bin size was 0.5 m, and data were collected with four pings per second. For stable data acquisition, the ship speed was maintained at an average of 4–5 knots, and real-time latitude and longitude data were obtained by connecting the global positioning system (GPS) to a laptop. The water temperature and salinity profiles were collected by a conductivity-temperature-depth (CTD, Idronaut Ocean Seven 304 Plus) sensors casting at a total of 14 positions (A1–A10 and B1–B5; note that B1 and A8 are the same positions).

Reliable signals within the ADCP ensemble were distinguished through a quality check and data processing protocol following Kim, Woo, and Kwon (2022). The velocity profile data exposed to the sea surface or missing GPS signals were discarded. The ADCP data showing pitch, roll, and head tilt of more than 8°, or percent good variable less than 90, were removed. Following the data processing methods described by Valle-Levinson

21699291, 2023, 5, Downloaded from https://agupubs.onlinelibrary.wiley.com/doi/10.1029/2022JC019338 by Inha University, Wiley Online Library on [11/03/2024]. See the Terms and Conditions (https://onlinelibrary.wiley.com/terms-and-conditions) on Wiley Online Library for rules of use; OA articles are governed by the applicable Creative Commons License

21699291, 2023, 5, Downloaded from https://agupubs.onlinelibrary.wiley.com/doi/10.1029/2022JC019338 by Inha University, Wiley Online Library on [11/03/2024]. See the Terms and Conditions (https://onlinelibrary.wiley.com/terms-and-conditions) on Wiley Online Library for rules of use; OA articles are governed by the applicable Creative Commons License

Table 1
Summary of Acoustic Doppler Current Profiler (ADCP) Surveys Conducted on 5 and 10 August 2011

Observation line	Observation time (hh:mm:ss)		Number of surveys	Mean survey duration (min)	Transect length (km)	Sampling rate (Hz)	Bin size (m)
A1–A7	Start	07:30:55	13	39.27	5.28	4	0.5
	End	19:30:53					
B5–B1(A8)–A10	Start	07:30:04	13	33.18	4.15	4	0.5
	End	19:30:56					

Note. Conductivity-temperature-depth observations along the ADCP survey lines were conducted at a total of 14 points, A1–A7 and B5–B1(A8)–A10.

and Atkinson (1999), we removed outliers that exceeded 2.5 standard deviations from the velocity profile, and performed linear interpolation for missing data using the nearest neighbor data. The compass and magnitude errors of the velocity derived from ship speed were corrected according to Joyce (1989). The three-point average method proposed by Dinehart and Burau (2005) was applied to prevent distortion of the velocity profile. The two observation lines were each divided into equal intervals of 20 m, and velocity ensembles within the range were averaged to reduce spatial signal deviations.

To reduce the calculation error between bins due to the tidal range, the σ-coordinate system that normalizes the observed depth by dividing with the total depth was used. The raw velocity components of u and v were converted into velocity components in σ-coordinate (u_σ and v_σ) with 81 equally spaced σ-levels indicating the velocity error before and after sigma coordinate conversion of less than 0.002 m s^{-1}, where $\sigma = d/D$; d is the water depth of each ADCP bin, and D is the maximum water depth at each ADCP data-position. Here, $\sigma = 0$ and $\sigma = 1$ are $d = 0$ (near-surface) and $d = D$ (near-bed), respectively. This coordinate transformation is a suitable method for calculating the residual circulation in a macrotidal estuary system (Giddings et al., 2014). The velocity results were converted into the along- and across-channel components.

The tide data for August 2011 were obtained from the Mokpo tide station of the Korea Hydrographic and Oceanographic Agency (KHOA) (Figure 3b). The tide level exhibited distinct spring-neap variations and the ebb-dominance was characterized with a long duration of a rising tide. For the amplitudes of S_2 and N_2, they are 4.8 times and 2.8 times lower than M_2, respectively (Table 2). The estuary dam discharged freshwater during all ebb current periods from August 7 to 14. Among these days, discharge was notable on August 10 (Figure 3c), when there were two discharges of approximately 2.88×10^3 m^3 s^{-1} and 3.58×10^3 m^3 s^{-1}. The first discharge occurred for approximately 4 hr from 2:26 to 6:23, and the second discharge was completed between 13:21 and 18:03. Although there was no discharge on August 15, the discharge of August 14 lasted till 20:35, approximately 10 hr before the start of observation.

3.2. Estimation of Along-Channel Residual Velocity

The observed velocity data included components of multiple harmonics and residual components in response to various external forcings. The separate effects of the different semidiurnal components (M_2, N_2, and S_2) could not be resolved as the observation period fell short of the Rayleigh criterion. Therefore, it is more correct to present them as tidal bands rather than natural harmonics. In this study, the residual velocity for the along-channel components was estimated using a least-squares fit (LSF) method on the semidiurnal, quarter-diurnal, and sixth diurnal tidal bands (D2, D4, and D6) (Lwiza et al., 1991) as follows:

$$u = u_0 + A_{D2}\sin(\omega_{D2}t + \phi_{D2}) + A_{D4}\sin(\omega_{D4}t + \phi_{D4}) + A_{D6}\sin(\omega_{D6}t + \phi_{D6}) \quad (1)$$

where, u and u_0 are the along-channel velocity and the along-channel residual velocity, respectively. t is time. A, ω, and ϕ, respectively, are the velocity amplitude, frequency, and phase, respectively, for the tidal constituents of D2, D4, and D6. The least-squares harmonic analysis was performed

Table 2
Harmonic Constants of the Five Major Constituents at Mokpo Tide Station (T1)

Constituents	Amplitude (m)	Phase (°)
M_2	1.44	38.18
S_2	0.50	87.88
K_1	0.31	250.40
O_1	0.24	217.77
N_2	0.30	18.63

21699291, 2023, 5, Downloaded from https://agupubs.onlinelibrary.wiley.com/doi/10.1029/2022JC019338 by Inha University, Wiley Online Library on [11/03/2024]. See the Terms and Conditions (https://onlinelibrary.wiley.com/terms-and-conditions) on Wiley Online Library for rules of use; OA articles are governed by the applicable Creative Commons License

Table 3
Statistical Analysis Results for Mean Error (ME), Mean Absolute Error (MAE), and Root Mean Square Error (RMSE) at A1, A5, A10, and B5

	LSF			S_TIDE		
	ME ($m\ s^{-1}$)	MAE ($m\ s^{-1}$)	RMSE ($m\ s^{-1}$)	ME ($m\ s^{-1}$)	MAE ($m\ s^{-1}$)	RMSE ($m\ s^{-1}$)
A1	−0.029	0.029	0.034	−0.026	0.026	0.032
A5	0.023	0.039	0.050	0.025	0.039	0.050
A10	−0.093	0.093	0.094	−0.089	0.089	0.091
B5	−0.004	0.041	0.051	0.003	0.052	0.082

independently for the time series of u_σ and v_σ at each bin. Because the data collection was performed for a short-term period of 13 hr, the length of the time series for the velocity at each bin was not sufficient to solve the diurnal tidal constituents. However, as a result of harmonic analysis of the water level at the Mokpo tide station, the sum of the amplitudes of K_1 and O_1 was less than 23% of the total tidal amplitude (Kang, 1999). Therefore, most of the residual dynamics of the Yeongsan River estuary can be sufficiently explained without considering diurnal tides.

The velocity data were additionally analyzed using the non-stationarity tidal analysis package (S_TIDE) (Pan et al., 2018) because the combination of the discharge period and the tidal period can result in non-stationarity (Matte et al., 2013) in the river-dominant estuary. To examine the performance of LSF and S_TIDE to along-channel velocity, the mean error (ME), mean absolute error (MAE), and root mean square error (RMSE) are calculated by the equations expressed as:

$$\mathrm{ME} = \frac{1}{N}\sum u_{\mathrm{obs}} - u_{\mathrm{LSF,\ S_TIDE}} \tag{2a}$$

$$\mathrm{MAE} = \frac{1}{N}\sum \left|u_{\mathrm{obs}} u_{\mathrm{LSF,\ S_TIDE}}\right| \tag{2b}$$

$$\mathrm{RMSE} = \sqrt{\frac{1}{N}\sum \left(u_{\mathrm{obs}} - u_{\mathrm{LSF,\ S_TIDE}}\right)^2} \tag{2c}$$

where N is the number of data. The obs denote the observation data. ME represents the bias of u_{LSF} and $u_{\mathrm{S_TIDE}}$ for u_{obs}. Since MAE represents the absolute value of the error between $u_{\mathrm{LSF,S_TIDE}}$ and u_{obs}. When the MAE and RMSE are low, the fit results for LSF and S_TIDE methods were reasonable. The ME, MAE, and RMSE results for A1, A5, A10, and B5 are shown in Table 3.

The u_{LSF} slightly underestimates the u_{obs} with 0.004–0.093 $m\ s^{-1}$ at A1, A10, and B5 and slightly overestimates the u_{obs} with 0.023 $m\ s^{-1}$ at A5. ME results for S_TIDE were slightly underestimated in A1 and A10, and slightly overestimated in A5 and B5. The magnitudes of the MAE and RMSE were similar for all four comparison points between LSF and S_TIDE. These error results show that the tidal current equation fitted using the least-squares method reflected the pattern of raw data well, resulting in the induced residuals producing a reliable representation of the actual conditions.

4. Results

4.1. Variations of Along-Channel Velocity

In this section, the total velocity variations observed in transects I and II are described. During non-discharge period, the velocity magnitude through transect II was stronger than that through transect I. The results of the along-channel velocity during the maxima flood and ebb currents, slack before flood, and slack before ebb without the freshwater discharge period are shown in Figure 4. In the regions adjacent to the estuary dam, almost all ebb currents below 0.2 $m\ s^{-1}$ were dominant, regardless of the tidal phase. During the maximum flood current (Figure 4; S5 period), the maximum current speed toward the estuary dam was observed at the southern end of transect II, and a relatively stronger flow occurred toward the estuary dam in the middle layer of the junction between transects I and II. The magnitude of the flood current weakened and became the ebb current on approaching the regions adjacent to the estuary dam. During the maximum ebb current (Figure 4; S12 period), the ebb current was predominantly observed in both transects I and II, and the maximum current speed was observed at the southern end of transect II equal to the maximum value position of the flood current.

During both slack periods, a velocity phase lag existed between the two channels. In the slack before ebb period (Figure 4; S9 period), the ebb current was maintained in the surface layer of transect II, but it turned into the flood current in the middle layer. During this period, the flow in the western part of transect I connected to the open sea, turned to flood current in the entire water column, while the flow in the eastern part of transect I changed to flood

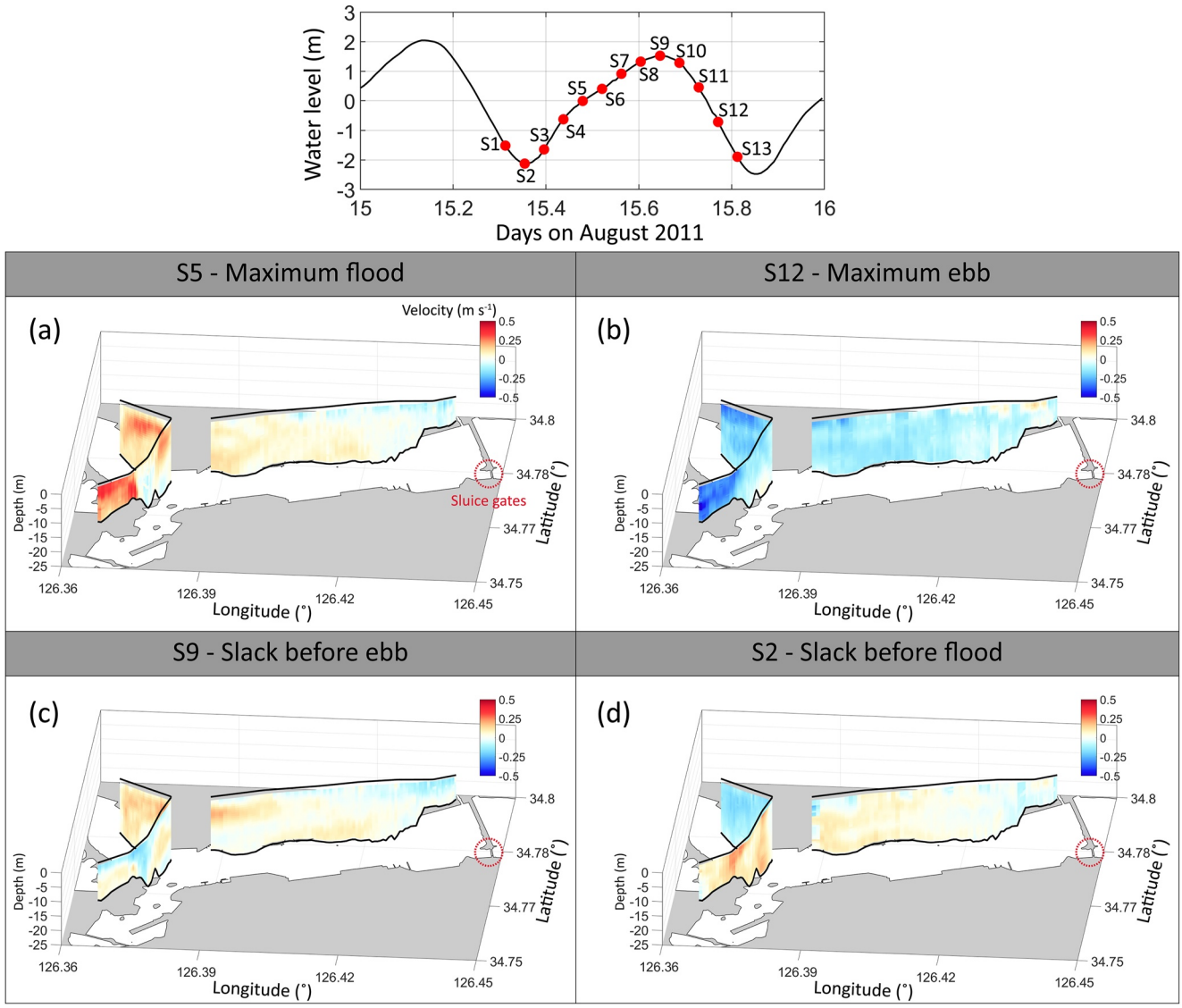


Figure 4. Along-channel velocity variations during non-discharge period on 15 August 2011: (a) maximum flood current, (b) maximum ebb current, (c) slack before ebb, and (d) slack before flood periods. The positive and negative values in the along-channel velocity indicate the flow toward the estuary dam and the open sea, respectively.

current only in the middle and near-bottom layers. During the slack before flood period (Figure 4; S2 period), the direction of tidal flow between the western and eastern parts of transect I were opposite. During this period, in transect II, the flood current prevailed over the entire water column.

A distinct increase in the velocity magnitude was observed in both transects I and II during the discharge period (Figure 5). During the maximum flood current period in the 1 hr after discharge (Figure 5; N3 period), an ebb current of 0.56 m s^{-1} was dominant within a distance of 5 m below the surface. The maximum velocity of the flood current was observed in the lower layer of the western part of transect I, while a weak flood current of less than 0.15 m s^{-1} was observed in the eastern part. In transect II, the flood current was observed at depths of 5–10 m, and the ebb current was dominant at depths below 10 m. During the periods of maximum ebb current and slack before flood (Figure 5; N9 and N11 periods), a strong ebb current of 1.5 m s^{-1} or more was observed within 10 m below the surface of the entire observation lines owing to the influence of freshwater discharge, whereas a flood current of 0.47 m s^{-1} or higher was observed in the lower layer. These results suggest that the strong discharge through the estuary dam does not directly affect the flow patterns at the lower layer. However, the flood currents can be induced in the lower layer through the entrainment of water due to velocity shear. Therefore,

21699291, 2023, 5, Downloaded from https://agupubs.onlinelibrary.wiley.com/doi/10.1029/2022JC019338 by Inha University, Wiley Online Library on [11/03/2024]. See the Terms and Conditions (https://onlinelibrary.wiley.com/terms-and-conditions) on Wiley Online Library for rules of use; OA articles are governed by the applicable Creative Commons License

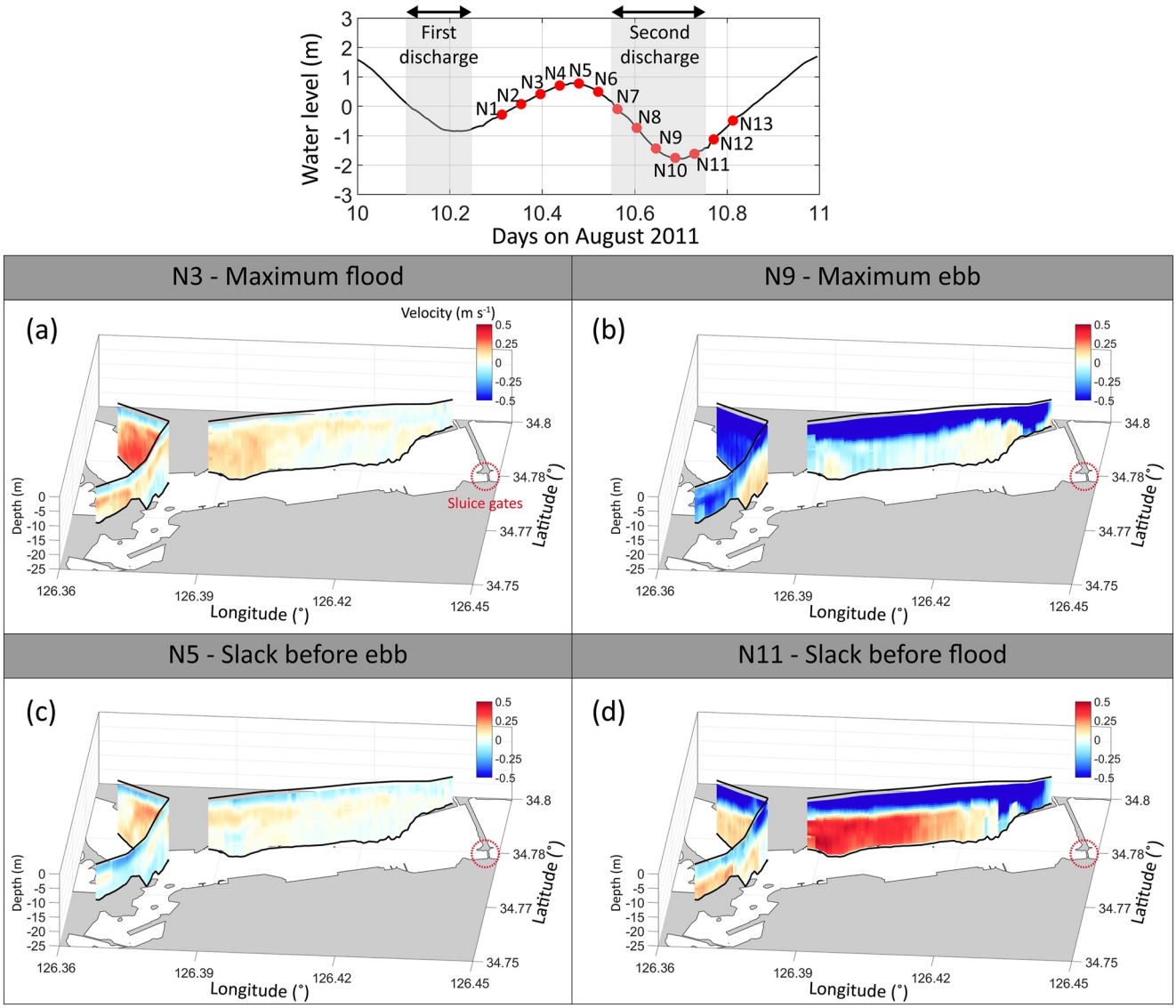


Figure 5. Along-channel velocity variations in the freshwater discharge period on 10 August 2011: (a) maximum flood current, (b) maximum ebb current, (c) slack before ebb, and (d) slack before flood periods. The positive and negative values in the along-channel velocity indicate the flow toward the estuary dam and the open sea, respectively.

near-bed mass transports toward the region adjacent to the estuary dam may be at a higher rate during discharge periods than during non-discharge times.

4.2. Salinity Variations

The spatiotemporal salinity variations observed during non-discharge periods are shown in Figure 6. In both transects I and II, a salinity of 15 or less were distributed at 0–5 m below the surface, and a relatively high salinity of 26–28 was observed at a depth of 7 m or less. The differences in salinity between the upper and lower layers over the entire observation period show that the discharge effect persists long, even 22 hr after the completion of the discharge. Particularly, the salinity in the surface layer of transect II increased by 5 or more with time, but there was little change in the surface salinity of transect I. This may be related to vertical mixing due to strong currents and increased velocity shear at the southern end of transect II. A weak velocity shear of less than 0.05 m s^{-1} was distributed throughout transect I, whereas at the southern end of transect II, the velocity shear reached a maximum of approximately 0.35 m s^{-1} during the maximum ebb current periods. Thus, the vertical mixing of salts in

21699291, 2023, 5, Downloaded from https://agupubs.onlinelibrary.wiley.com/doi/10.1029/2022JC019338 by Inha University, Wiley Online Library on [11/03/2024]. See the Terms and Conditions (https://onlinelibrary.wiley.com/terms-and-conditions) on Wiley Online Library for rules of use; OA articles are governed by the applicable Creative Commons License

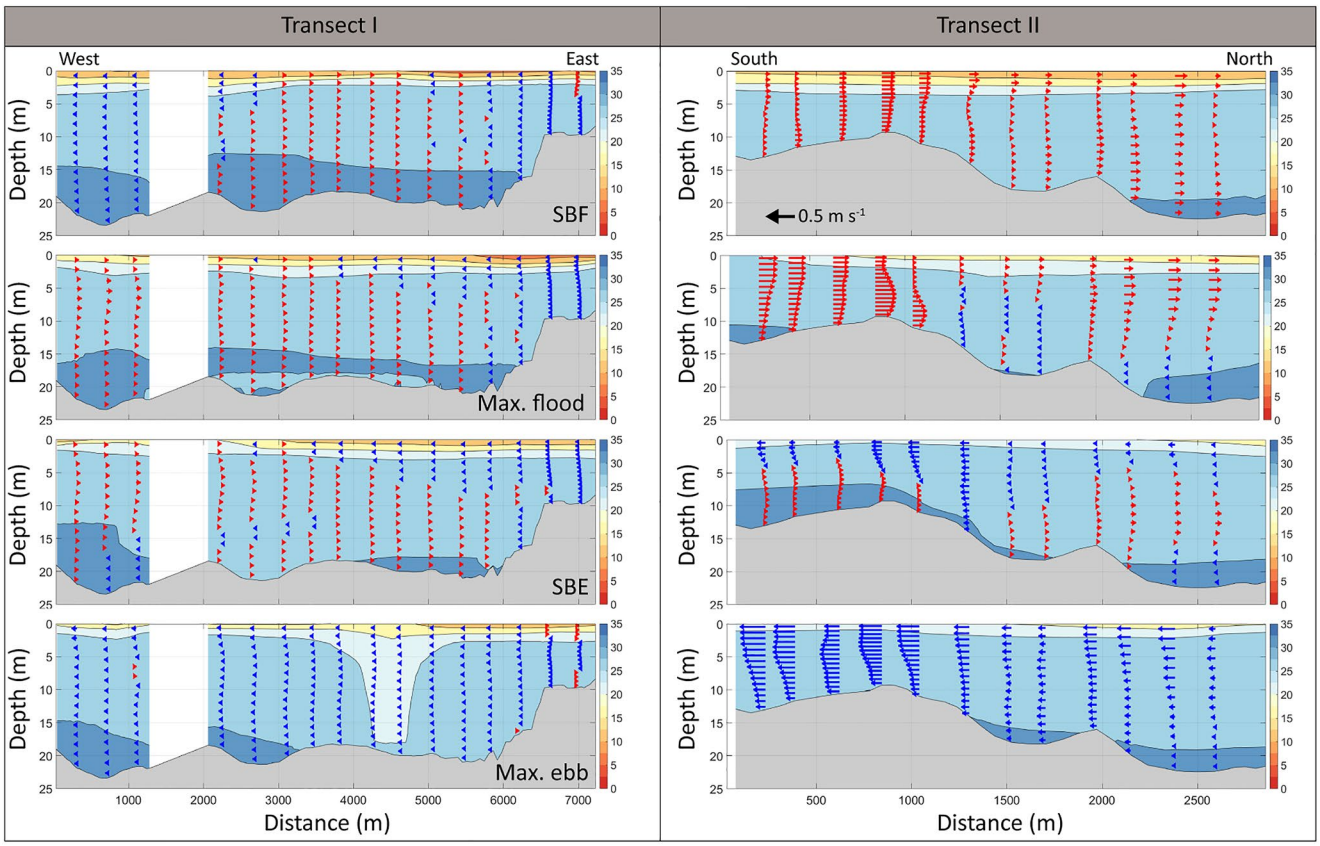


Figure 6. Salinity variations during non-discharge period on 15 August 2011. The red and blue arrows indicate the along-channel flow toward the estuary dam and the open sea, respectively.

the inner part of the Yeongsan River estuary mainly occurs through the velocity shear of transect II rather than that of transect I.

During the discharge period (Figure 7), low salinity of 0–10 was observed within 3 m below the surface during the maximum flood current due to the impact of discharge that occurred 1 hr before the start of observation in both transects I and II. The salinity distributions during the slack periods before ebb and that before the maximum flood current periods were similar, and the salinity in transect I was lower than that in transect II. During the maximum ebb current and slack periods before the flood currents at the time of discharge, the freshwater was spread horizontally in a range of approximately 6 km from the vicinity of the estuary dam to the junction of transect II, and a salinity of less than 20 was observed vertically to a depth of 12 m. Moreover, during these periods, the maximum current speed occurred near the estuary dam of transect I, but the horizontal velocity gradient and velocity shear were highest at the northern part of transect II. Importantly, to compensate for the water volume that escaped through the surface layer momentarily due to the discharge, the velocity intensity of discharge toward the estuary dam and salinity value at the bottom layer were strengthened. These results suggest that freshwater discharge can be a major driving force for mass transport toward the estuary dam, because the flood current in the vicinity of the dam was weak during the non-discharge period.

4.3. Residual Flow Patterns

The along-channel residual flow pattern during non-discharge period exhibited a complex multi-layer vertical structure at transect I (Figure 8a). A negative residual velocity of 0.05 m s^{-1} or less was predominant over the entire water column at a depth of 10 m adjacent to the estuary dam located at the eastern end of transect I. As the water depth rapidly deepened to 20 m and more, the residual velocity toward the open sea within the depth of 0–4 m was still observed, whereas residual velocities toward the estuary dam within the depth of 4–12 m and 15–20 m were dominant. The residual flow of transect I toward the estuary dam at 4–12 m depth was strongly

21699291, 2023, 5, Downloaded from https://agupubs.onlinelibrary.wiley.com/doi/10.1029/2022JC019338 by Inha University, Wiley Online Library on [11/03/2024]. See the Terms and Conditions (https://onlinelibrary.wiley.com/terms-and-conditions) on Wiley Online Library for rules of use; OA articles are governed by the applicable Creative Commons License

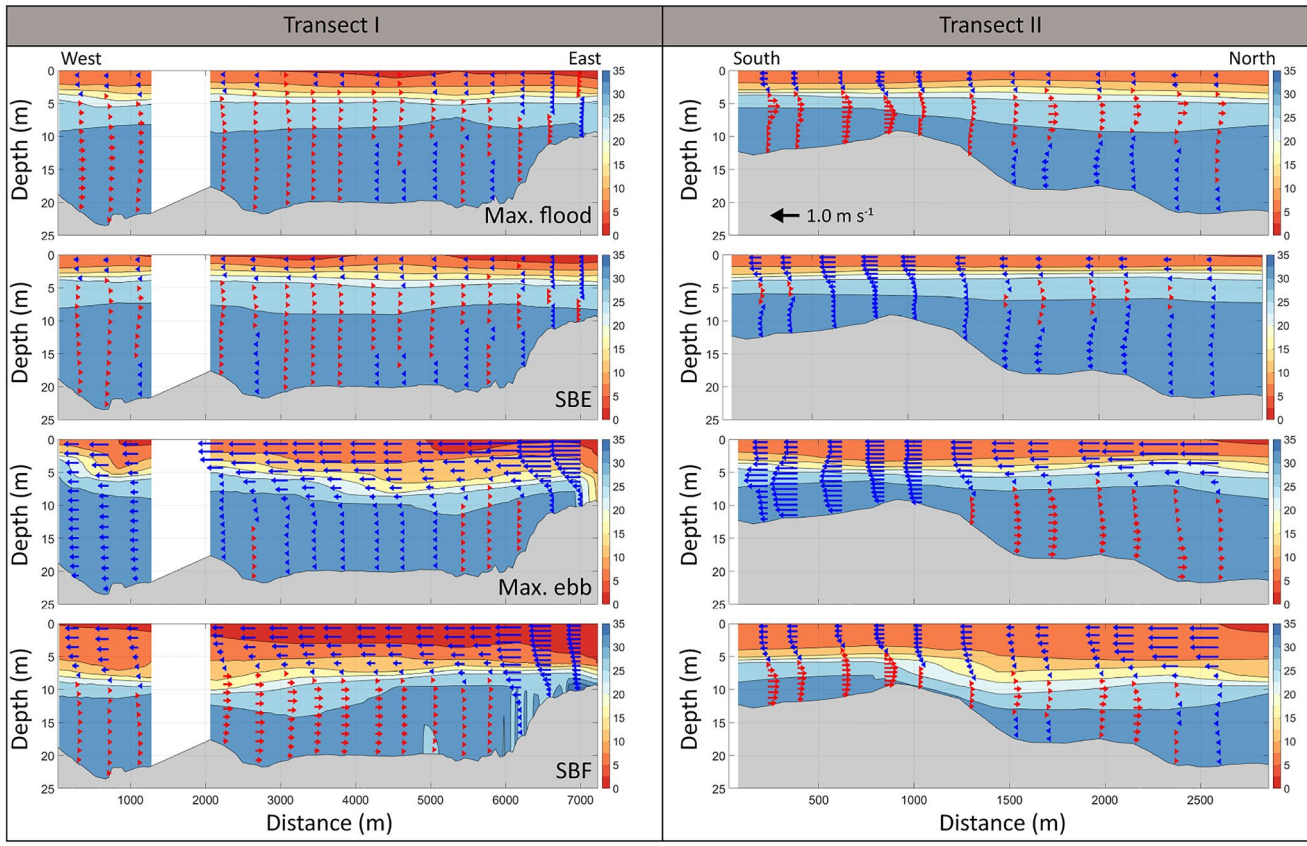


Figure 7. Salinity variations related to freshwater discharge on 10 August 2011. During the maximum ebb current and slack before flood periods, direct freshwater discharge from the estuary dam occurred. The red and blue arrows indicate the along-channel flow toward the estuary dam and the open sea, respectively.

influenced by the mid-layer flow in the western part, whereas the same at 15–20 m depth can be attributed to the induction of flow at the left and right of the bottom layer at the northern end of transect II. In transect II, the residual velocity was partially negative at the center of the channel, but the positive flow, mainly toward the estuary dam, was dominant. The intensity of residual flow in transect II was stronger than that in transect I. Eventually, the positive residual flow of transect II is a structure that flows into transect I, and the flow insertion process from this lateral direction can contribute to the formation of a multi-layer vertical structure in transect I.

During the discharge period (Figure 8b), a distinct two-layer vertical structure of along-channel residual flow was observed in transect I, different from that observed during non-discharge period. In transect I, negative residual velocities of approximately 0.4 m s^{-1} or more were distributed within the water depths of 10 m, whereas positive residual velocity was dominant at a depth of less than 10 m, with a maximum of 0.15 m s^{-1}. The two-layer estuarine exchange processes can supply the salt near the bottom layer toward the estuary dam. Therefore, the long-term salt budget inside the Yeongsan River estuary is maintained by the competition between salt loss due to the controlled-discharge from the dam and salt increase due to the estuarine exchange flow. The negative residual velocity was observed within a water depth of 5 m in transect II, similar to the surface residual velocity intensity of transect I. On the contrary, unlike the positive velocity of transect I, the residual velocity of transect II in the bottom layer was mainly observed as negative except for that at the northern part. These results for the residual velocity suggest that the effect of freshwater discharge induces not only the outflux of materials toward the open sea on the surface layer, but also the transport of materials from the bottom layer to the estuary dam because of the high-velocity shear. As the intensity of residual velocity observed during discharge was more than twice that during non-discharge, net material circulation between the open sea and the inner part of the estuary in the summer season can be determined by the presence or absence of freshwater discharge.

21699291, 2023, 5, Downloaded from https://agupubs.onlinelibrary.wiley.com/doi/10.1029/2022JC019338 by Inha University, Wiley Online Library on [11/03/2024]. See the Terms and Conditions (https://onlinelibrary.wiley.com/terms-and-conditions) on Wiley Online Library for rules of use; OA articles are governed by the applicable Creative Commons License

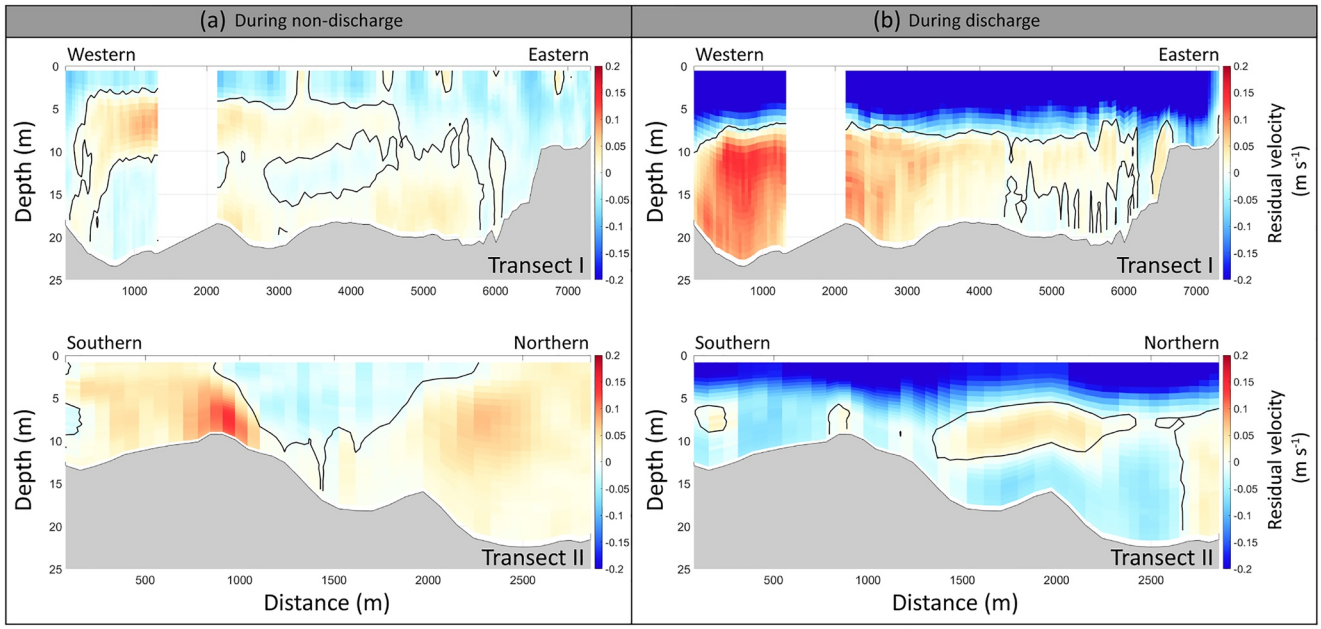


Figure 8. Along-channel residual velocity profiles at transects I and II during (a) non-discharge and (b) discharge periods. Positive and negative values indicate residual flow toward the estuary dam and open sea, respectively.

5. Discussion

5.1. Nonlinear Effects Associated With Channel Topography

The residual flow patterns in transects I and II exhibited different patterns in response to the presence or absence of freshwater discharge and the resulting flow interaction between the two channels. Here, the interaction of strong tidal currents with narrow width, shallow water depth, and shoal of transect II can produce nonlinear effects such as flow acceleration owing to overtides associated with bottom friction (Xu et al., 2021). Furthermore, because the velocity intensity in transect I was weaker than that in transect II during non-discharge, and the water depth was constant, the nonlinear effects in transect II may be more important to the overall residual circulation system in the inner part of the Yeongsan River estuary.

To examine the nonlinear effects associated with the topographic structure, the velocity distributions of the amplitudes of the D2, D4, and D6 tidal constituents were observed during non-discharge period, as shown in Figure 9. In transect I, the distribution of D2 amplitude exhibited the highest velocity of 0.25 m s^{-1} around the surface in the upper 5 m of the western part of the channel, and this velocity tended to weaken as it approached the eastern end of the channel. The velocity decreased overall with the water depth, but at a distance of 2,200–5,000 m in transect I, the velocity at the bottom layer was higher than that at the surface layer. In this region of the transect, at a depth of 5–10 m, the velocity at D2 amplitude was less than 0.1 m s^{-1}, which was relatively low compared with the surface and bottom layers, but the velocity at D4 amplitude reached approximately 0.06 m s^{-1}. The highest velocity at D4 amplitude in transect I was approximately 0.08 m s^{-1} at a depth of 15–20 m in the western part, comparable to that at D2 amplitude. The velocity at D6 amplitude was less than 0.02 m s^{-1} over the entire transect I region. However, this value was comparable to those at the D2 and D4 amplitudes at the eastern end of the transect.

In transect II, the distribution pattern of overtides was largely divided into two regions, the southern and northern parts, based on the central shoal. In the southern part of transect II, the highest velocity of 0.3 m s^{-1} at D2 amplitude was distributed at a distance of 0–1,000 m. Over the entire region, the velocity at D2 amplitude generally decreased with water depth, but velocities of 0.3 m s^{-1} were confined to near-beds only in the shoal region (distance of approximately 900 m). These high values (>0.25 m s^{-1}) decreased as the water depth increased toward the northern part of transect II. In the northern part, a velocity of more than 0.2 m s^{-1} at D2 amplitude was observed in the upper layer adjacent to a distance of 2,400 m, while a relatively low velocity of 0.08 m s^{-1} or less was observed at the lower layer. The velocity at D4 amplitude in the southern

21699291, 2023, 5, Downloaded from https://agupubs.onlinelibrary.wiley.com/doi/10.1029/2022JC019338 by Inha University, Wiley Online Library on [11/03/2024]. See the Terms and Conditions (https://onlinelibrary.wiley.com/terms-and-conditions) on Wiley Online Library for rules of use; OA articles are governed by the applicable Creative Commons License

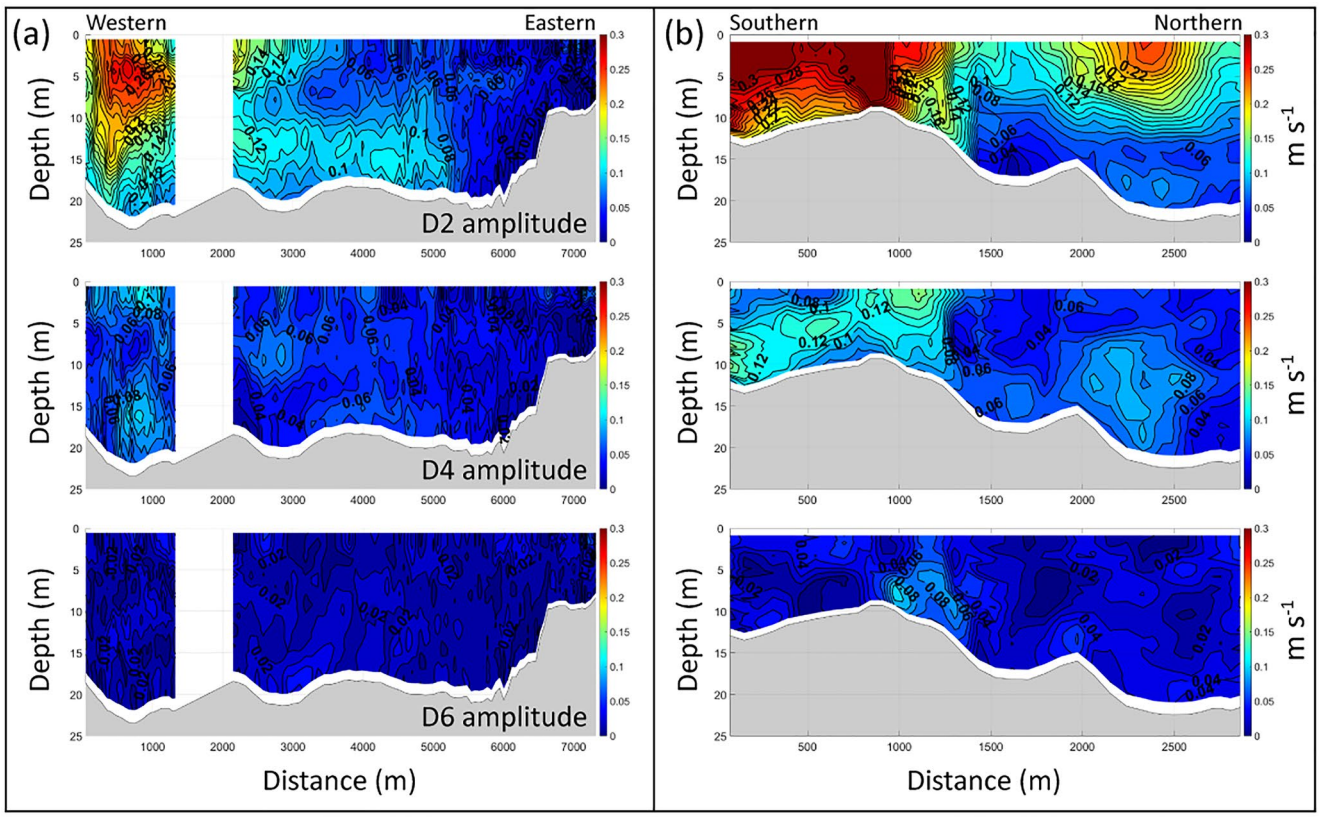


Figure 9. Comparison of the along-channel tidal amplitude distributions for the D2, D4, and D6 between transects (a) I and (b) II.

part was half that at D2 amplitude, whereas the velocity at D4 amplitude in the bottom layer of the northern part reached about 0.08 m s^{-1}, which was higher than that at D2 amplitude. In addition, the highest velocity of 0.08 m s^{-1} at D6 amplitude was observed to be comparable with the velocities at D2 and D4 amplitudes in the shoal region.

Overall, the velocities at D4 and D6 amplitudes near the intersection of transects I and II were high enough to be compared to those at D2 amplitude. This suggests that different tidal current patterns through the two channels intersected at the bifurcated channel point, resulting in flow acceleration related to an increase in nonlinear effects. To compare the intensity of nonlinearity between transects I and II, the ratio of D4 and D2 amplitudes (D4/D2) was calculated during the period without freshwater discharge. The larger this ratio, the more likely the residual flow is the result of nonlinearity (Friedrichs & Aubrey, 1988).

In transect I, the D4/D2 amplitude ratio was clearly largest on the steep slope where water depth rapidly changed (distance of 5,500–7,300 m) near the estuary dam (Figure 10). Over this distance range, the ratio was 1 near the surface and bottom layers, but showed a low ratio of less than 0.2 partially at a water depth of 5 m. A maximum ratio of 0.6 was observed at a depth of 5–10 m at 2,200–5,000 m distance. A ratio of 0.6 or more near a distance of 1,000 m along transect I was strongly related to the high nonlinearity strength in the bottom layer at a distance of 1,300–3,000 m along transect II. Therefore, the multi-layer vertical structure of residual velocity at the channel bifurcation point during the non-discharge period may be attributed to the nonlinearity effect of the spatial velocity gradient between two channels. At the amplitude of the overtides observed in the mesotidal estuary systems, the D4 amplitude was approximately thrice the value of the D6 amplitude (Le Provost & Forferino, 1985). However, results similar to ours, that is, reports of high proportions of D4 and D6 to D2 are rare. This increase in D6 amplitude, as well as D4 amplitude, suggests that there may be significant causes that were less relevant in other systems, such as horizontal friction. The occurrence of a D6 amplitude similar to the D4 amplitude and the observed residual flow pattern indicates the importance of friction on momentum balance, which is further discussed in the next section dealing with the along-channel dynamics.

21699291, 2023, 5, Downloaded from https://agupubs.onlinelibrary.wiley.com/doi/10.1029/2022JC019338 by Inha University, Wiley Online Library on [11/03/2024]. See the Terms and Conditions (https://onlinelibrary.wiley.com/terms-and-conditions) on Wiley Online Library for rules of use; OA articles are governed by the applicable Creative Commons License

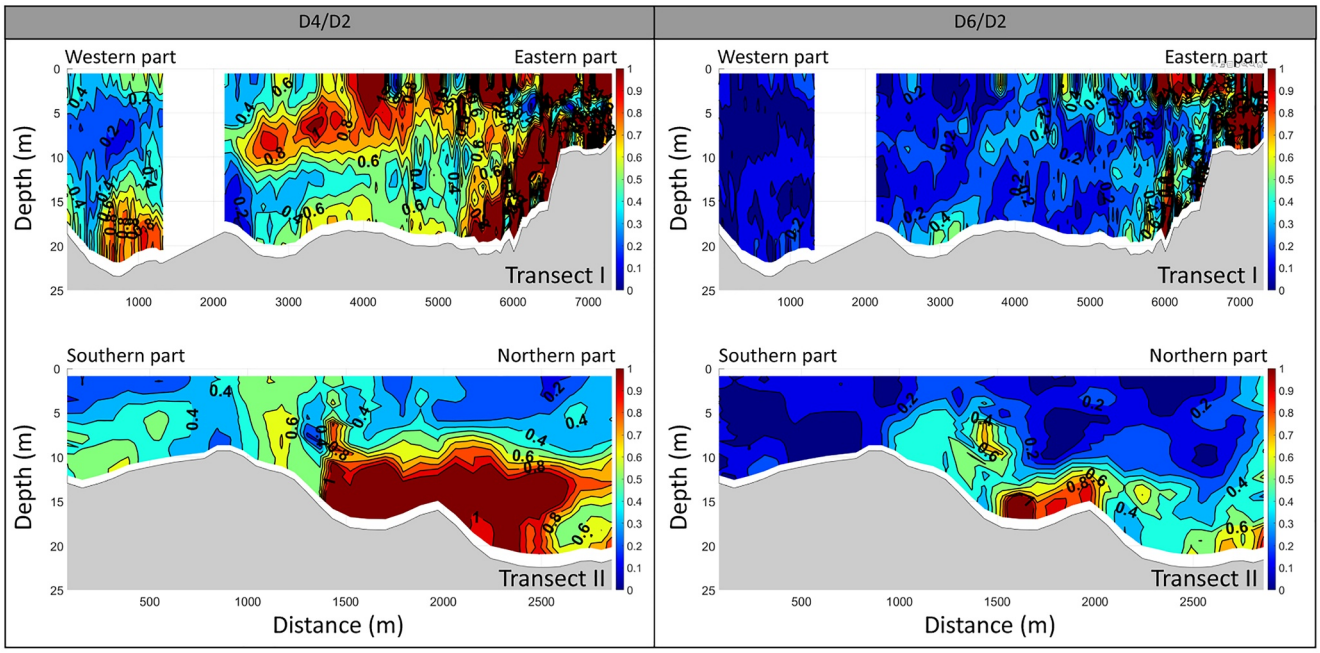


Figure 10. Comparisons of the D4/D2 and D6/D2 ratios between transects I and II.

5.2. Along-Channel Momentum Dynamics

In the inner part of the Yeongsan River estuary, during the non-discharge period, the magnitudes of overtides were strongest in the steeply sloping area near the estuary dam and at the channel junction. This overtide was usually derived from nonlinear effects related to the terms of advection acceleration and friction (Parker, 1991). To examine the relative importance of advection and friction effects on the residual circulation in the inner part of the Yeongsan River estuary, the along-channel momentum balance was estimated. Assuming a steady state, inhomogeneity, nonlinearity, and vertical and horizontal frictions in the along-channel direction, the residual momentum balance can be expressed as follows (Cáceres et al., 2003):

$$\left\langle u\frac{\partial u}{\partial x}\right\rangle - \langle fv\rangle = -\left\langle \frac{1}{\rho_0}\frac{\partial p}{\partial x}\right\rangle + \left\langle A_z\left(\frac{\partial^2 u}{\partial z^2}\right)\right\rangle + \left\langle A_h\left(\frac{\partial^2 u}{\partial x^2}\right)\right\rangle \quad (3)$$

where the $u(\partial u/\partial x)$ is the advective term, fv is the Coriolis term ($f = 8.32 \times 10^{-5}$ s^{-1}), $1/\rho_0(\partial p/\partial x)$ is the pressure gradient term, ρ_0 is tidally and depth-averaged density, and $A_z(\partial^2 u/\partial z^2)$ and $A_h(\partial^2 u/\partial x^2)$ are the vertical and horizontal frictional terms, respectively. The brackets denote the temporal average over a tidal cycle. In this study, only the baroclinic pressure gradient term was considered as the term related to the pressure gradient. This is because baroclinic pressure gradient ($\left\langle \frac{g}{\rho_0} z\frac{\partial \rho}{\partial x}\right\rangle \approx 5.36 \times 10^{-5}$: $g = 9.8$ m s^{-2}; $z = 20$ m; $\partial\rho = 2.04$ kg m^{-3}; $\partial x = 7{,}290$ m; $\rho_0 = 1{,}024$ kg m^{-3}) is one order of magnitude higher than barotropic pressure gradient ($\left\langle g\frac{\partial \eta}{\partial x}\right\rangle \approx 8.07 \times 10^{-6}$: $\partial\eta = 0.006$ m) between A1 and 10. The water level slope ($\partial\eta$) was determined from the de-meaned and detrended time series of the CTD pressure sensors at A1 and A10.

The A_z is the vertical eddy viscosity, estimated in the empirical form $A_z = 0.01(1 + 5Ri)^{-2} + 10^{-4}$ (Pacanowski & Philander, 1981; Valle-Levinson et al., 2000), where the Ri is the Richardson number. The equation is dependent on spatially-temporarily varying Ri and is suitable for application in areas where the mixing process can be influenced by strong residual shear due to strong freshwater discharge. Throughout the spring and neap tide, the A_z value varied from 5 to 24 $\times 10^{-4}$ m^2 s^{-1}, and relatively low values distributed around 5–10 m of water depth associated with the stratification. A_h is the horizontal viscosity estimated using the empirical form $A_h = A_z(\Delta x/h_0)^2$ proposed by Ianniello (1979), where Δx and h_0 are the width and maximum water depth of the channel, respectively. The equation of Ianniello (1979) is applicable in shallow estuary regions ($h/b < 1$; h is maximum water depth and b is channel width) where the channel widths of less than 1–2 km and horizontal friction can

21699291, 2023, 5, Downloaded from https://agupubs.onlinelibrary.wiley.com/doi/10.1029/2022JC019338 by Inha University, Wiley Online Library on [11/03/2024]. See the Terms and Conditions (https://onlinelibrary.wiley.com/terms-and-conditions) on Wiley Online Library for rules of use; OA articles are governed by the applicable Creative Commons License

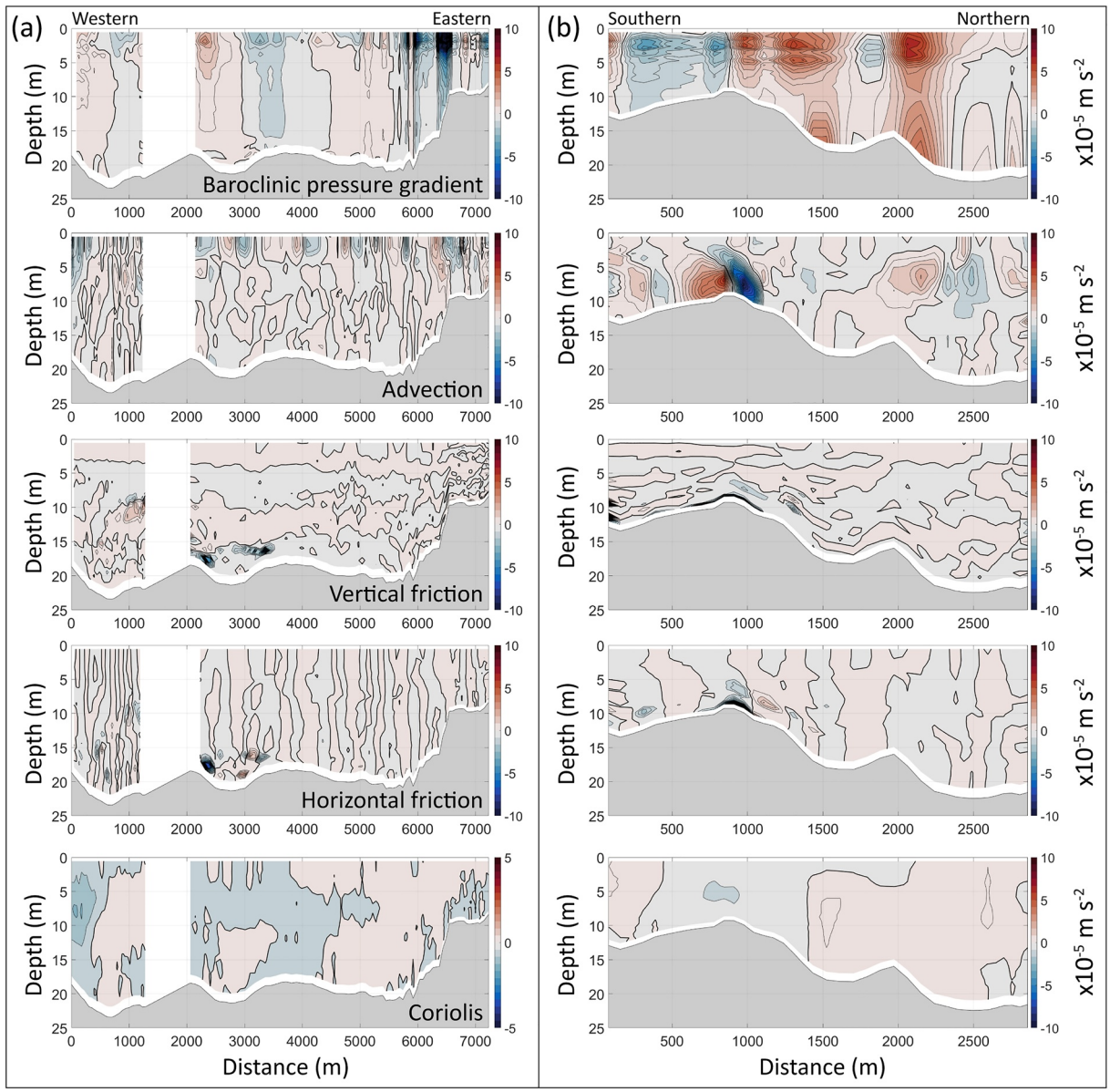


Figure 11. Along-channel momentum balances during non-discharge period between transects (a) I and (b) II on 15 August 2011.

become as important as vertical friction. Since the width of the Yeongsan River estuary is within 1–2 km and the depth of the water is less than 20 m, In this study, A_h was estimated based on this equation.

During the non-discharge period, the residual flow patterns at the channel junction of transect I were presented as a multi-layered vertical structure toward the open sea at depths of 5 m and 10–15 m, and toward the dam at depths of 5–10 m and 15–20 m. Here, the along-channel residual flow toward the open sea within 5 m of the surface may have been induced by an advection term in which the largest scale in the same water depth is consistently distributed (Figure 11a). The advection term, which was relatively higher than that at the bottom layer, was mainly distributed within 5 m of the surface, and the highest magnitude of the advection term was estimated near the estuary dam. This is consistent with the distribution of the high estimated D4/D2 and D6/D2 ratios in the surface layer near the estuary dam. Moreover, the highest magnitude of the vertical friction term was estimated at the mid-layer of the bifurcation of transects I and II. The residual flow toward the estuary dam within 5–10 m of the channel junction may be due to the vertical friction term. For both horizontal friction and Coriolis terms, the highest values were estimated at the western end of transect I. The increase in the magnitude of rotational

21699291, 2023, 5, Downloaded from https://agupubs.onlinelibrary.wiley.com/doi/10.1029/2022JC019338 by Inha University, Wiley Online Library on [11/03/2024]. See the Terms and Conditions (https://onlinelibrary.wiley.com/terms-and-conditions) on Wiley Online Library for rules of use; OA articles are governed by the applicable Creative Commons License

21699291, 2023, 5, Downloaded from https://agupubs.onlinelibrary.wiley.com/doi/10.1029/2022JC019338 by Inha University, Wiley Online Library on [11/03/2024]. See the Terms and Conditions (https://onlinelibrary.wiley.com/terms-and-conditions) on Wiley Online Library for rules of use; OA articles are governed by the applicable Creative Commons License

motion and horizontal friction at the western end may be due to the curved channel structure. The cross-sectional mean values for the absolute values of baroclinic pressure gradient, advection, vertical friction horizontal friction, and Coriolis terms were 5.70, 2.67, 1.17, 0.93, and 1.14×10^{-6} m s^{-2}, respectively. The sum of the friction and advection terms was comparable to the baroclinic pressure term, and relative to the other four terms, the nonlinear effect of advection is the major contributor to the momentum balance.

In transect II (Figure 11b), the momentum balance varied significantly in the vicinity of the water slope area at a distance of 800–2,000 m. In particular, the highest magnitude was estimated around a distance of 1,000 m for all four terms, and this distribution was the same as the distribution of the maximum residual flow in transect II. In addition, at a distance of 1,500–2,500 m, where the ratio of overtides was high, the magnitude of advection and horizontal friction terms was more than twice the other two terms. The cross-sectional mean values for the absolute values of baroclinic pressure gradient, advection, vertical friction horizontal friction, and Coriolis terms were 12.72, 7.15, 5.79, 1.74, and 2.26×10^{-6} m s^{-2}, respectively. Like transect I, the dominant term balanced with the baroclinic pressure gradient term in transect II was the advection term. Overall, the momentum terms of transect II were larger than those of transect I. The highest term in balance with pressure gradient term was the advection term out of four terms, similar to that in transect I, but unlike in transect I, the horizontal friction term of transect II was almost equal in magnitude to the vertical friction term. Therefore, it can be a controlling factor in the residual circulation in the inner part of the Yeongsan River estuary due to the nonlinearity effect related to the horizontal friction of transect II during non-discharge period.

The major mechanism of momentum balance during the discharge period is the vertical friction term (Figure 12). As mentioned in Section 2, this change in the momentum balance mechanism is important in terms of residual circulation because the discharge from the estuary dam was mostly continuous during the summer season. In transect I, the magnitude of the horizontal friction term as well as the vertical friction term was larger than that of the advection term. Most friction terms with high magnitude were distributed within 5 m, whereas high advection terms were distributed up to approximately 10 m. These distributions were similar to residual flow patterns within 10 m below the water surface during the discharge. In the case of transect II, the vertical friction term was also the largest among the momentum balance terms. High intensities of terms for the advection, vertical and horizontal frictions were mainly observed in the surface layer. Only the horizontal friction term had high intensity observed in the lower layer at the northern end of transect II. The cross-sectional mean values of the baroclinic pressure gradient, advection, vertical and horizontal frictions, and Coriolis terms in transect I were 157.22, 38.83, 91.59, 43.38, and 3.46×10^{-6} m s^{-2}, respectively, while the respective values in transect II were 47.01, 19.35, 25.99, 21.34, and 3.07×10^{-6} m s^{-2}. Therefore, during the discharge period, the frictional terms contribute more to the momentum balance than the advection term, and it is remarkable that they are distinct from the major mechanisms during non-discharge period.

Residual momentum balances in the along-channel dynamics were mainly expressed in terms of tidal averaged horizontal pressure gradients and vertical shear stresses (Kim & Voulgaris, 2005). Nevertheless, this balance can be modified by the nonlinearities arising from various sources, such as bottom friction, tidal asymmetry, and complex bathymetry condition. In particular, on steep slopes of the water depth, shoal region, and bifurcated channel, geometrical properties may be highly relevant as they can create advection accelerations associated with the along-channel momentum balances. The findings of this study indicate that the bathymetric structure of the channel and the increase in the nonlinearity of the horizontal friction term associated with the freshwater discharge play an important role in driving the residual circulation, and their contribution may be much greater than the advection and vertical friction terms along the channel. In addition, the major mechanism of momentum balance between the discharge and non-discharge periods is related to many other phenomena such as increased residence time, accumulation of substances, and development of hypoxia at the Yeongsan River estuary (Lim & Park, 1998). We expect that these factors also contribute majorly to the material circulation.

The residual dynamics analysis using the LSF contains several uncertainties. First, the calculated residual component includes diurnal tidal effects that cannot be resolved due to the length of the data. As reported by Bang et al. (2013), the diurnal (K_1 and O_1) tidal current amplitudes at the outer region (approximately 15 km westward from A10) of the Yeongsan River estuary were 0.08 and 0.07 m s^{-1}, respectively, and the sum of these values was approximately 15% of the sum of the semi-diurnal tidal current. Although the reported results differ in observation period and location from this study, the influence of diurnal tides may affect residual circulation. Another uncertainty of the tidal analysis is the non-stationarity. As shown in Table 3, in the tidal analysis using

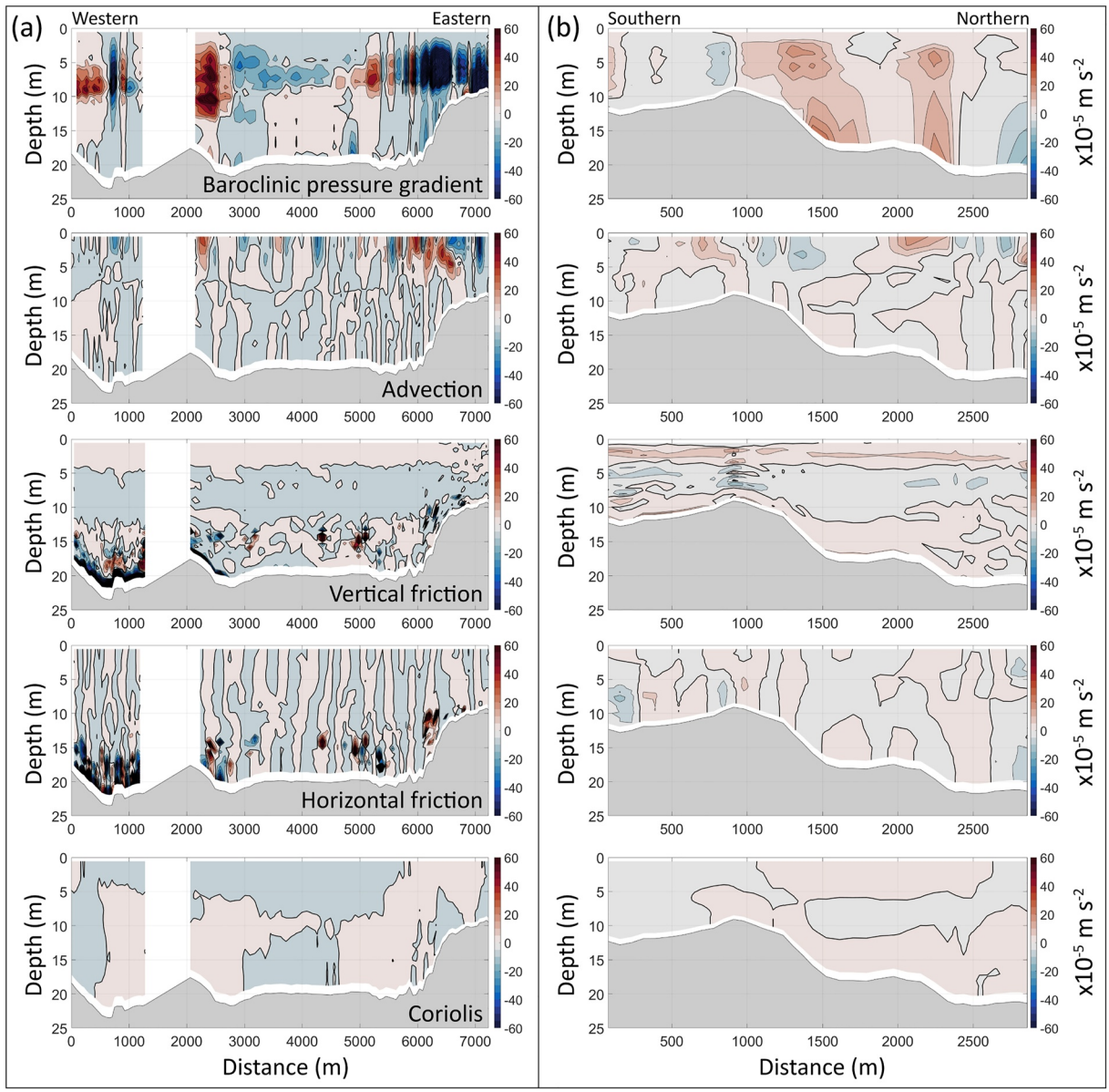


Figure 12. Along-channel momentum balances with the freshwater discharge period between transects (a) I and (b) II on 10 August 2011.

LSF and S_TIDE, there was little difference in RMSE between the two methods in A1, A5, and A10 of transect I (<0.03 m s^{-1}), while the difference in RMSE between the two methods in B5 of transect II was about 0.3 m s^{-1}. These results suggest that tidal forcings in transect II are more highly fluctuated by the freshwater discharge than in transect I, and the resulting non-stationarity can significantly affect residual flows. The LSF method has been applied for spatial residual circulation analysis in various estuaries as well as this study, and the aforementioned uncertainties have been supplemented through long-term monitoring data or numerical modeling. Therefore, we expect that this observational study on the residual circulation in the inner part of the Yeongsan River estuary will be discussed in more detail and contribute to new findings in subsequent studies.

6. Conclusions

The Yeongsan River estuary has been greatly affected by the freshwater discharge from an estuary dam installed to secure freshwater sources and prevent flooding. Freshwater discharge plays an important role in the residual circulation structure in bifurcated channels, and it is necessary to fully understand its mechanisms between

21699291, 2023, 5, Downloaded from https://agupubs.onlinelibrary.wiley.com/doi/10.1029/2022JC019338 by Inha University, Wiley Online Library on [11/03/2024]. See the Terms and Conditions (https://onlinelibrary.wiley.com/terms-and-conditions) on Wiley Online Library for rules of use; OA articles are governed by the applicable Creative Commons License

21699291, 2023, 5, Downloaded from https://agupubs.onlinelibrary.wiley.com/doi/10.1029/2022JC019338 by Inha University, Wiley Online Library on [11/03/2024]. See the Terms and Conditions (https://onlinelibrary.wiley.com/terms-and-conditions) on Wiley Online Library for rules of use; OA articles are governed by the applicable Creative Commons License

channels through proper monitoring. In this study, field observations were performed at the inner part of the Yeongsan River estuary to analyze the residual flow structure and its mechanisms in the main channel, transect I, and the subchannel, transect II, which were affected by the freshwater discharge. The following conclusions are drawn from this study:

(1) During the non-discharge period, meaningful changes in the hydrodynamics of the inner part of the estuary occurred in transect II rather than transect I. The magnitudes of the maximum flood and ebb currents in transect II were greater than those in transect I. In addition, the velocity shear in transect II was 1.3 times greater than that in transect I. The low salinity of 15 or less remaining in the surface layer did not change in transect I over time, whereas in transect II, it increased by more than five, which was related to the velocity shear in transect II.

(2) During the discharge period, the change in the hydrodynamics in transect I was greater than that in transect II. A distinct jet-like-flow with a velocity of more than 1.5 m s^{-1} toward the open sea and a salinity close to zero was observed within the top 12 m of the water column in transect I. At the same time, a current flow toward the estuary dam at the bottom layer was significantly developed in transect I with a velocity of 0.47 m s^{-1} or higher. However, in transect II, a jet-like-flow toward the open sea within the top 5 m of the water column was developed similarly to that of transect I, but salinity changes in transect II were insignificant. These results suggest that the freshwater discharge effect of the estuary has a limited effect on transect I, and the residual circulation between the two channels and its major mechanism may be different.

(3) For the residual flow of transect I, a multi-layer vertical structure was observed during the non-discharge period, whereas a two-layer vertical structure was observed during the discharge period. The multi-layer vertical structure of transect I during the non-discharge period was attributed to the residual flow of the bottom layer introduced from transect II. During discharge, the surface and bottom layers were clearly divided into two layers due to the effect of freshwater discharge, but flow exchange through the bottom layer between transects I and II was insignificant.

(4) The highest overtides of D4 and D6 associated with bottom friction were distributed on the steep slope, where water depth rapidly changed, adjacent to the estuary dam of transect I. In addition, D4/D2 ratios at the western end of transect I, which were greater than 0.5, were highly associated with overtides formed in the shoal region of transect II. The development of these overtides indicates domination of nonlinear effects during the absence of freshwater discharge from the estuary dam, and hence, the nonlinear acceleration term may be the major mechanism behind momentum balance.

(5) The major mechanisms of along-channel momentum balance with and without freshwater discharge were completely different. During non-discharge period, the advection term was most dominant, whereas the vertical friction term was most dominant during the discharge period. It is noteworthy that the horizontal friction term, as well as the vertical friction term, was relatively larger than the advection term during the discharge period. Therefore, controlled discharges from the estuary dam can determine the major mechanism underlying the residual flow dynamics of the estuary system. The installation of marine infrastructure on various coastlines is increasing; hence, our research results provide a good example for the future identification of the causes of environmental changes.

Data Availability Statement

The observational data and codes of tide level, ADCP and CTD used in this paper are available in the Zenodo database (Kim, Woo, Song, & Yoon, 2022, https://doi.org/10.5281/zenodo.7084833).

Acknowledgments
This research was supported by the Basic Science Research Program through the National Research Foundation of Korea (NRF) funded by the Ministry of Education (NRF-2021R1I1A1A01060397). This research was also supported by a National Research Foundation of Korea Grant from the Korean Government (MSIT; the Ministry of Science and ICT) (NRF-2021M1A5A1075516) (KOPRI-PN23013).

References

Aubrey, D., & Speer, P. E. (1985). A study of non-linear tidal propagation in shallow inlet/estuarine systems Part I: Observations. *Estuarine, Coastal and Shelf Science*, *21*(2), 185–205. https://doi.org/10.1016/0272-7714(85)90096-4

Bang, K.-Y., Kim, T. I., Song, Y. S., Lee, J. H., Kim, S. W., Cho, J.-G., et al. (2013). Numerical modeling of sediment transport during the 2011 summer flood in the Youngsan River Estuary, Korea. *Journal of Korean Society of Coastal and Ocean Engineers*, *25*(2), 76–93. https://doi.org/10.9765/KSCOE.2013.25.2.76

Buschman, F. A., Hoitink, A. J. F., van der Vegt, M., & Hoekstra, P. (2010). Subtidal flow division at a shallow tidal junction. *Water Resources Research*, *46*(12), W12515. https://doi.org/10.1029/2010WR009266

Cáceres, M., Valle-Levinson, A., & Atkinson, L. (2003). Observations of cross-channel structure of flow in an energetic tidal channel. *Journal of Geophysical Research*, *108*(C4), 3114. https://doi.org/10.1029/2001JC000968

Chen, S. N., Sanford, L. P., & Ralston, D. K. (2009). Lateral circulation and sediment transport driven by axial winds in an idealized, partially mixed estuary. *Journal of Geophysical Research*, *114*(C12), C12006. https://doi.org/10.1029/2008JC005014

Cho, Y.-K., Park, L.-H., Cho, C., Lee, I. T., Park, K.-Y., & Oh, C.-W. (2004). Multi-layer structure in the Youngsan Estuary, Korea. *Estuarine, Coastal and Shelf Science*, *61*(2), 325–329. https://doi.org/10.1016/j.ecss.2004.06.003

Dinehart, R. L., & Burau, J. R. (2005). Averaged indicators of secondary flow in repeated acoustic Doppler current profiler crossings of bends. *Water Resources Research*, *41*(9), W09405. https://doi.org/10.1029/2005WR00405

Dyer, K. (1997). *Estuaries, a physical introduction* (2nd ed.). Wiley.

Friedrichs, C. T., & Aubrey, D. G. (1988). Non-linear tidal distortion in shallow well-mixed estuaries: A synthesis. *Estuarine, Coastal and Shelf Science*, *27*(5), 521–545. https://doi.org/10.1016/0272-7714(88)90082-0

Geyer, W. R., Trowbridge, J. H., & Bowen, M. M. (2000). The dynamics of a partially mixed estuary. *Journal of Physical Oceanography*, *30*(8), 2035–2048. https://doi.org/10.1175/1520-0485(2000)030<2035:TDOAPM>2.0.CO;2

Giddings, S. N., Monismith, S. G., Fong, D. A., & Stacey, M. T. (2014). Using depth-normalized coordinates to examine mass transport residual circulation in estuaries with large tidal amplitude relative to the mean depth. *Journal of Physical Oceanography*, *44*(1), 128–148. https://doi.org/10.1175/JPO-D-12-0201.1

Hansen, D. V., & Rattray, M. (1965). Gravitational circulation in straits and estuaries. *Journal of Marine Research*, *23*, 104–122. Retrieved from https://images.peabody.yale.edu/publications/jmr/jmr23-02-06.pdf

Huijts, K. M. H., Schuttelaars, H. M., de Swart, H. E., & Friedrichs, C. T. (2009). Analytical study of the transverse distribution of along-channel and transverse residual flows in tidal estuaries. *Continental Shelf Research*, *29*(1), 89–100. https://doi.org/10.1016/j.csr.2007.09.007

Ianniello, J. P. (1979). Tidally induced residual currents in estuaries of variable breadth and depth. *Journal of Physical Oceanography*, *9*(5), 962–974. https://doi.org/10.1175/1520-0485(1979)009<0962:TIRCIE>2.0.CO;2

Joyce, T. M. (1989). On in situ "Calibration" of shipboard ADCPs. *Journal of Atmospheric and Oceanic Technology*, *6*(1), 169–172. https://doi.org/10.1175/1520-0426(1989)006<0169:OISOSA>2.0.CO;2

Kang, J. W. (1999). Changes in tidal characteristics as a result of the construction of sea-dike/sea-walls in the Mokpo coastal zone in Korea. *Estuarine, Coastal and Shelf Science*, *48*(4), 429–438. https://doi.org/10.1006/ecss.1998.0464

Kästner, K., & Hoitink, A. J. F. (2019). Flow and suspended sediment division at two highly asymmetric bifurcations in a river delta: Implications for channel stability. *Journal of Geophysical Research: Earth Surface*, *124*(10), 2358–2380. https://doi.org/10.1029/2018JF004994

Kim, J. W., Woo, S.-B., & Kwon, H.-K. (2022). An observational study of hydrodynamic impact on water mass transport due to tidal power generation. *Science of the Total Environment*, *807*, 151013. https://doi.org/10.1016/j.scitotenv.2021.151013

Kim, J. W., Woo, S.-B., Song, J. I., & Yoon, B. I. (2022). Effect of freshwater discharge from estuary dam on residual circulation in bifurcated channel (Version 1) [Dataset]. Zenodo. https://doi.org/10.5281/zenodo.7084833

Kim, Y. H., Hong, S., Song, Y. S., Lee, H., Kim, H.-C., Ryu, J., et al. (2017). Seasonal variability of estuarine dynamics due to freshwater discharge and its influence on biological productivity in Yeongsan River Estuary, Korea. *Chemosphere*, *181*, 390–399. https://doi.org/10.1016/j.chemosphere.2017.04.085

Kim, Y. H., & Voulgaris, G. (2005). Effect of channel bifurcation on residual estuarine circulation: Winyah Bay, South Carolina. *Estuarine, Coastal and Shelf Science*, *65*(4), 671–686. https://doi.org/10.1016/j.ecss.2005.07.004

Lacy, J. R., Stacey, M. T., Burau, J. R., & Monismith, S. G. (2003). Interaction of lateral baroclinic forcing and turbulence in an estuary. *Journal of Geophysical Research*, *108*(C3), 3089. https://doi.org/10.1029/2002JC001392

Le Provost, C., & Forferino, M. (1985). Tidal spectroscopy of the English Channel with a numerical model. *Journal of Physical Oceanography*, *15*(8), 1009–1031. https://doi.org/10.1175/1520-0485(1985)015<1008:TSOTEC>2.0.CO;2

Lim, H. S., & Park, K. H. (1998). Community structure of the macrobenthos in the soft bottom of Youngsan River estuary, KOREA 2. The occurrence of summer hypoxia and benthic community. *Journal of Korean Fishery Society*, *31*, 343–352. Retrieved from https://koreascience.kr/article/JAKO199823607632703.page

Lwiza, K. M. M., Bowers, D. G., & Simpson, J. H. (1991). Residual and tidal flow at a tidal mixing front in the North Sea. *Continental Shelf Research*, *11*(11), 1379–1395. https://doi.org/10.1016/0278-4343(91)90041-4

Matte, P., Jay, D. A., & Zaron, E. D. (2013). Adaptation of classical tidal harmonic analysis to nonstationary tides, with application to river tides. *Journal of Atmospheric and Oceanic Technology*, *30*(3), 569–589. https://doi.org/10.1175/JTECH-D-12-00016.1

Pacanowski, R. C., & Philander, S. G. H. (1981). Parameterization of vertical mixing in numerical models of tropical oceans. *Journal of Physical Oceanography*, *11*, 1443–1451. https://doi.org/10.1175/1520-0485(1981)011<1443:POVMIN>2.0.CO;2

Pan, H., Lv, X., Wang, Y., Matte, P., Chen, H., & Jin, G. (2018). Exploration of tidal-fluvial interaction in the Columbia River estuary using S_TIDE. *Journal of Geophysical Research: Ocean*, *123*(9), 6598–6619. https://doi.org/10.1029/2018JC014146

Park, L.-H., Cho, Y.-K., Cho, C., Sun, Y.-J., & Park, K.-Y. (2001). Hydrography and circulation in the Youngsan River estuary in summer, 2000. *The Sea Journal of the Korean Society of Oceanography*, *6*(4), 218–224. Retrieved from https://scienceon.kisti.re.kr/srch/selectPORSrchArticle.do?cn=JAKO200120417585138

Parker, B. B. (1991). The relative importance of the various nonlinear mechanisms in a wide range of tidal interactions. In B. B. Parker (Ed.), *Tidal hydrodynamics* (pp. 237–268). John Wiley.

Shan, S., Hannah, C. G., & Wu, Y. (2019). Coupling of estuarine circulations in a network of fjords. *Journal of Geophysical Research: Oceans*, *124*(10), 6809–6830. https://doi.org/10.1029/2018JC014924

Trowbridge, J. H., Geyer, W. R., Bowen, M. M., & Williams, A. J. (1999). Near-bottom turbulence measurements in a partially mixed estuary: Turbulent energy balance, velocity structure, and along-channel momentum balance. *Journal of Physical Oceanography*, *29*(12), 3056–3072. https://doi.org/10.1175/1520-0485(1999)029<3056:NBTMIA>2.0.CO;2

Valle-Levinson, A., & Atkinson, L. P. (1999). Spatial gradients in the flow over an estuarine channel. *Estuaries*, *22*(2), 179–193. https://doi.org/10.2307/1352975

Valle-Levinson, A., Wong, K., & Lwiza, K. M. M. (2000). Fortnightly variability in the transverse dynamics of a coastal plain estuary. *Journal of Geophysical Research: Ocean*, *105*(C2), 3413–3424. https://doi.org/10.1029/1999JC900307

Wu, Y., Xu, C., Ke, Y., Chen, K., & Xu, H. (2017). Multi-criteria decision-making on assessment of proposed tidal barrage schemes in terms of environmental impacts. *Marine Pollution Bulletin*, *125*(1–2), 271–281. https://doi.org/10.1016/j.marpolbul.2017.08.030

Xu, H., Shen, J., Wang, D., Luo, L., & Hong, B. (2021). Nonlinearity of subtidal estuarine circulation in the Pearl River estuary, China. *Frontiers in Marine Science*, *8*, 629403. https://doi.org/10.3389/fmars.2021.629403

Zhang, W., Feng, H., Hoitink, A. J. F., Zhu, Y., Gong, F., & Zheng, J. (2017). Tidal impacts on the subtidal flow division at the main bifurcation in the Yangtze River Delta. *Estuarine, Coastal and Shelf Science*, *196*, 301–314. https://doi.org/10.1016/j.ecss.2017.07.008

21699291, 2023, 5, Downloaded from https://agupubs.onlinelibrary.wiley.com/doi/10.1029/2022JC019338 by Inha University, Wiley Online Library on [11/03/2024]. See the Terms and Conditions (https://onlinelibrary.wiley.com/terms-and-conditions) on Wiley Online Library for rules of use; OA articles are governed by the applicable Creative Commons License